CHAPTER 3

MULTI-APERTURE SPECKLE INTERFEROMETRY FOR DEFORMATION MEASUREMENT

3.1 INTRODUCTION

Various methods in speckle interferometry have been reported for the measurement of deformation vectors. For in-plane displacement measurements either the Leendertz's two beam illumination method (Leendertz 1970) or Duffy's two aperture arrangement (Duffy 1972, 1974) is used. For out-of-plane displacement measurement, a reference wave is added at the image plane of the imaging lens either by using a small ground glass reference diffuser in one of the apertures (Mohanty et al. 1984) or by providing a smooth reference wave at the image plane (Adams and Maddux 1974). The recent interest in speckle interferometry lies in the extraction both these displacement components from a single experimental setup. As discussed in Section 1.4.2.4, aperturing of the lens is the obvious choice and offers several advantages; recording of several information on the same photographic plate and retrieval; simultaneous recording of both displacement and its derivatives; and enhancement of the contrast of the fringes. The aim of this chapter is to implement this aperturing concept in speckle interferometry for the simultaneous measurement of in-plane and out-of-plane displacement components of a deformation vector with comparable sensitivities.

3.2 SIMULTANEOUS MEASUREMENT OF IN-PLANE AND OUT-OF-PLANE DISPLACEMENT COMPONENTS

Numerous techniques in speckle interferometry have been reported for simultaneously measuring all the three components of a deformation vector. Adam and Maddux (1974) and Chandra Shakher and Sirohi (1978) combined holography and speckle photography to obtain out-of-plane and in-plane components of a displacement from a holospecklegram. Wu and Chiang (1986) used sandwich holo-speckle interferometry for measuring 3-D displacement fields near the blunt notch. Sirohi and Krishna Mohan (1992a) have measured all the three components of a deformation vector by multi-aperture speckle interferometry. This configuration is similar to that of Duffy's method but differs in that it uses five apertures instead of two apertures in front of the imaging lens in order to extract the u, v, and w components of the deformation vector. However, in this configuration, the sensitivity of measuring the in-plane displacement is poor and is equal to that of Duffy's method. This sensitivity is very less when compared to that of the Leendertz method. This section proposes a technique using multi-aperture arrangement to achieve comparable sensitivities for measuring both out-of-plane and in-plane displacement components of a deformation vector. The technique combines the out-of-plane sensitive configuration proposed earlier by Mohanty et al. (1984) with the combined Leendertz and Duffy's method of the in-plane sensitive configuration discussed in Section 2.3 of Chapter 2. The experimental arrangement and the detailed theory are discussed in the following sections.

3.2.1 Experimental arrangement

The experimental arrangement for the simultaneous measurement of in-plane and out-of-plane displacements with comparable sensitivities is shown in Figure 3.1.

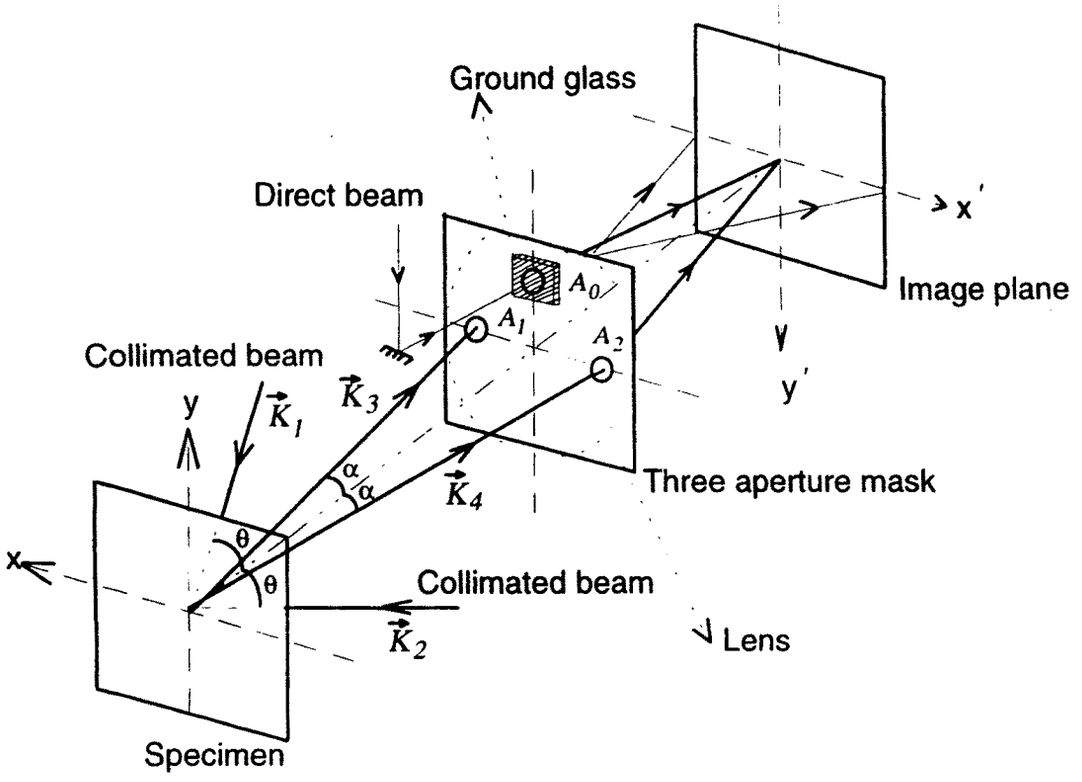

Figure 3.1 Experimental arrangement for the simultaneous measurement of in-plane and out-of-plane displacements

The object is illuminated by two collimated beams that are incident at an angle θ on either side of the optical axis. The imaging lens carries a mask containing three apertures. Aperture A_0 has a ground glass mounted on it. The ground glass plate is illuminated by a portion of the direct beam, and hence generates a diffuse reference beam at the image plane. The remaining two apertures A_1 and A_2 are used for image formation. Four beams, two through the apertures A_1 and A_2 due to the illumination beam having propagation vector $\vec{K}_1$ and the other two through the same apertures due to the illumination beam having propagation vector $\vec{K}_2$, combine coherently at the image plane.

3.2.2 Theory

The amplitude distribution at any point on the image plane can be written as

$$A_1 = a_0\, e^{i(\phi_0+\gamma)} + \sum_{m=1}^{2}\left\{ a_{2m-1}\, e^{i(\phi_{2m-1})} + a_{2m}\, e^{i(\phi_{2m}+\beta)} \right\}, \qquad (3.1)$$

where a,s and ϕs are the random amplitudes and phases of the waves generated from the illuminating beams via the apertures. The phases β and γ are responsible for the grating like structure in each speckle and are defined as $\beta = 2\pi\mu x$ and $\gamma = 2\pi\mu y$. The intensity distribution in the image plane is thus given by

$$\begin{aligned} I_1 = {} & \sum_{m=0}^{4}|a_m|^2 + 2\sum_{m=1}^{3} a_m a_{m+1}\cos\left(\phi_{m,m+1}+\beta\right) + 2a_1 a_4 \cos\left(\phi_{41}+\beta\right) \\ & + 2\sum_{m=1}^{2} a_m a_{m+2}\cos\left(\phi_{m,m+2}\right) + 2a_0 \sum_{m=1}^{2} a_{2m-1}\cos\left(\phi_{0,2m-1}+\gamma\right) \\ & + a_{2m}\cos\left(\phi_{0,2m}+\gamma-\beta\right), \end{aligned} \qquad (3.2)$$

where $\phi_{ij} = \phi_i - \phi_j$

When the object is loaded, the phases of the waves via the outer apertures A_1 and A_2 change. The amplitude distribution of the waves at the same point after deformation of the object is given by

$$A_2 = a_0\, e^{i(\phi_0+\gamma)} + \sum_{m=1}^{2}\left\{ a_{2m-1}\, e^{i\left(\phi_{2m-1}+\vec{\delta}_{2m-1}\right)} + a_{2m}\, e^{i\left(\phi_{2m}+\vec{\delta}_{2m}+\beta\right)} \right\}, \qquad (3.3)$$

where $\vec{\delta}$s are the phase changes introduced due to the object deformation. The phase changes which can be expressed in terms of directions of illumination and directions of observation are defined in Equation (2.16) of Chapter 2.

The intensity distribution at the image plane after the object deformation is given by

$$I_2 = \sum_{m=0}^{4} |a_m|^2 + 2\sum_{m=1}^{3} a_m a_{m+1} \cos\left(\phi_{m,m+1} + \vec{\delta}_{m,m+1} + \beta\right) + 2a_1 a_4 \cos\left(\phi_{41} + \vec{\delta}_{41} + \beta\right)$$
$$+ 2\sum_{m=1}^{2} a_m a_{m+2} \cos\left(\phi_{m,m+2} + \vec{\delta}_{m,m+2}\right) + 2a_0 \sum_{m=1}^{2} a_{2m-1} \cos\left(\phi_{0,2m-1} + \vec{\delta}_{2m-1} + \gamma\right)$$
$$+ a_{2m} \cos\left(\phi_{0,2m} + \vec{\delta}_{2m} + \gamma - \beta\right) \qquad (3.4)$$

The intensity distribution I_1 and I_2 are sequentially recorded on the same photographic plate. Assuming linear recording, the amplitude transmittance t(x,y) of the specklegram is given by Equation (2.6) of Chapter 2.

To obtain correlation fringes, the specklegram is placed in the whole-field filtering setup as shown in Figure 1.5 of Chapter 1. At the focal plane of the lens L_1 seven diffraction halos are formed. Figure 3.2 shows the schematic representation of these diffraction halos and the corresponding phase terms associated with these halos.

3.2.3 Fringe analysis

a) In-plane displacement measurement

The information filtered via any one of the diffraction halos A_{12} can be used for the measurement of the in-plane displacement component. The intensity distribution in the image formed via halo A_{12} is given by Equation (2.18) of Chapter 2 and the rest of the theory related to this in-plane displacement measurement is the same as that discussed in Sections 2.3.3 and 2.3.4 of Chapter 2. This analysis clearly shows that the sensitivity using this method is considerably increased for the measurement of the in-plane displacement component compared to earlier techniques

(Adams and Maddux 1974, Chandra Shakher and Sirohi 1978 and Sirohi and Krishna Mohan 1992).

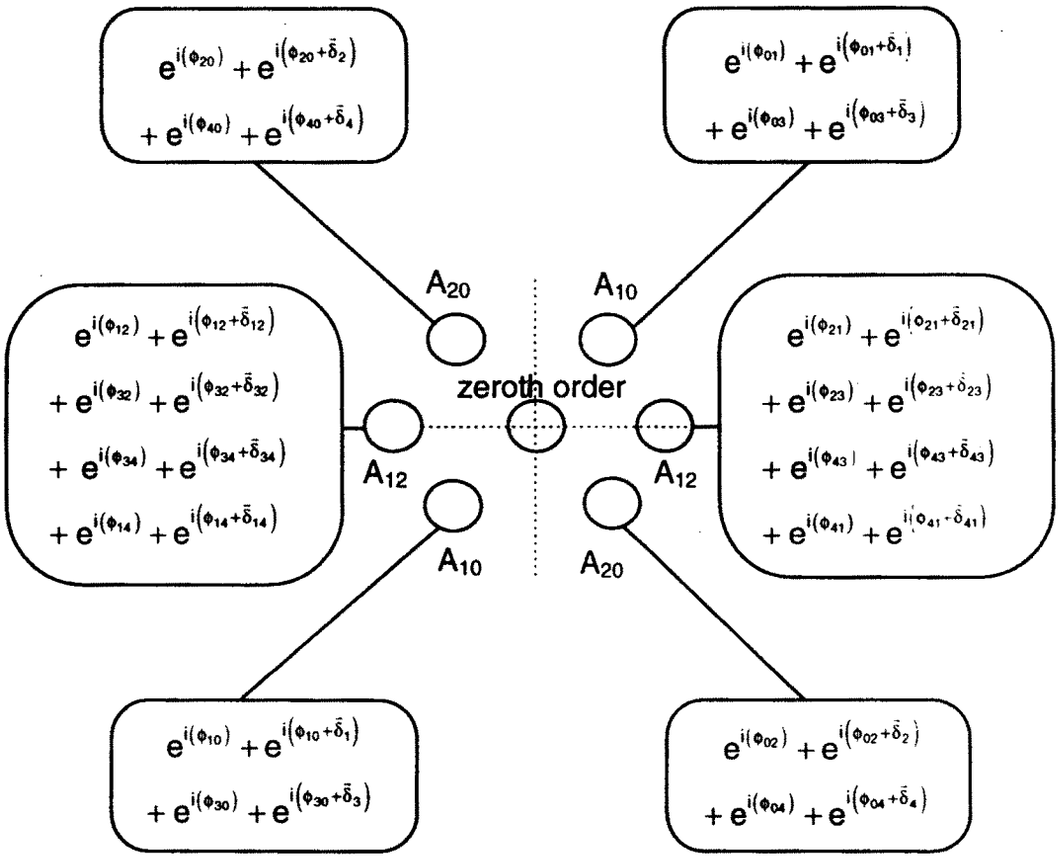

Figure 3.2 Arrangement of phase terms in Fourier transform plane

b) Out-of-plane displacement measurement

The information filtered via any one of the diffraction halos A_{10} or A_{20} can be used for the measurement of out-of-plane displacement. The intensity distribution in the interferogram formed via the halos A_{10} and A_{20} are given by

$$I_{(A_{10})} = c'\left[4+2\cos\phi+2\cos\left(\phi-\vec{\delta}_1\right)+2\cos\left(\phi+\vec{\delta}_3\right)+2\cos\left(\phi+\vec{\delta}_3-\vec{\delta}_1\right)\right.$$

$$\left.+2\cos\vec{\delta}_1+2\cos\vec{\delta}_3\right] \qquad (3.5)$$

and

$$I_{(A_{20})} = c''\left[4+2\cos\phi'+2\cos\left(\phi'-\vec{\delta}_2\right)+2\cos\left(\phi'+\vec{\delta}_4\right)+2\cos\left(\phi'+\vec{\delta}_4-\vec{\delta}_2\right)\right.$$

$$\left.+2\cos\vec{\delta}_2+2\cos\vec{\delta}_4\right], \qquad (3.6)$$

where

$$\phi = \phi_{03} - \phi_{01} \quad \text{and} \quad \phi' = \phi_{04} - \phi_{02}\,.$$

It may be seen that the terms containing ϕ and ϕ' generate a speckled texture to the image. We thus obtain fringe patterns corresponding to $\vec{\delta}_1$ and $\vec{\delta}_3$ that are modulated by $\cos\left[\left(\vec{\delta}_3-\vec{\delta}_1\right)/2\right]$, via the halo A_{10}, which is the moiré pattern. Similarly fringes are formed corresponding to $\vec{\delta}_2$ and $\vec{\delta}_4$ which are modulated by the $\cos\left[\left(\vec{\delta}_4-\vec{\delta}_2\right)/2\right]$ term via halo A_{20}.

Assuming that the illuminating beams lie in the x–z plane, we can express the phase changes $\vec{\delta}_1$ and $\vec{\delta}_3$ that are responsible for fringe formation via halo A_{10} as

$$\vec{\delta}_1 = \frac{2\pi}{\lambda}\left[u(\sin\theta-\sin\alpha)+w(\cos\alpha+\cos\theta)\right] = 2m_1'\pi\,,$$

$$\vec{\delta}_3 = \frac{2\pi}{\lambda}\left[u(-\sin\theta-\sin\alpha)+w(\cos\alpha+\cos\theta)\right] = 2m_2'\pi\,. \qquad (3.7)$$

Similarly the phase changes $\vec{\delta}_2$ and $\vec{\delta}_4$ that are responsible for fringe formation via the halo A_{20} can be expresses as

$$\vec{\delta}_2 = \frac{2\pi}{\lambda}\left[u(\sin\theta+\sin\alpha)+w(\cos\alpha+\cos\theta)\right] = 2m_1''\pi$$

$$\vec{\delta}_4 = \frac{2\pi}{\lambda}\left[u(-\sin\theta+\sin\alpha)+w(\cos\alpha+\cos\theta)\right] = 2m_2''\pi \qquad (3.8)$$

It can be observed from the Equations (3.7) and (3.8) that the fringe patterns obtained via the halos A_{10} and A_{20} differ by the negative sign associated with $\sin\alpha$. Here the angle α is governed by the aperture separation and the distance between the lens and the object and is usually very small compared to the angle of illumination. Therefore under this assumption the filtered images via halos A_{10} and A_{20} are identical and are governed by

$$u\sin\theta + (1+\cos\theta)w = m_1\lambda, \tag{3.9}$$

$$-u\sin\theta + (1+\cos\theta)w = m_2\lambda. \tag{3.10}$$

A beat between these two set of fringe patterns results in a moiré pattern that represents only the in-plane displacement component. The fringe spacing corresponds to an incremental displacement of $\lambda/2\sin\theta$ which is the same as that of the information obtained from halo A_{12} (Equation 2.2.3 of Chapter 2). This in-plane displacement component (u) can be used to measure the out-of-plane displacement component (w) from the fringe pattern (Equations (3.9) and (3.10)) (Krishna Mohan et al. 1994).

3.2.4 Experimental results

The experiments are conducted on a centrally loaded diaphragm with the edges rigidly clamped. The diaphragm is fabricated from a phosphor bronze sheet (0.7 mm thickness and a diameter of 60 mm) and is coated with aluminium paint. The diaphragm is fixed on a precision rotary stage provided with a micrometer head at the center. The diaphragm is simultaneously subjected to in-plane rotation and out-of-plane deflection. The specimen is illuminated with two collimated beams at an angle of 20° on either side of the surface normal from a 25 mW He–Ne laser. A standard camera lens (f=150 mm, f/5.6) is used for imaging the specimen onto the recording medium. A three aperture mask is placed in front of the imaging lens. The middle aperture A_0 which has a ground glass plate mounted on it

is illuminated by a portion of the direct beam. The ground glass plate is used for providing a uniform reference beam over the whole image at the image plane. The other two apertures A_1 and A_2 are used for imaging. Two exposures, one before and the other after the loading of the object are made on a 10E75 holographic plate. The specimen is given an in-plane rotation of about 0.45 mrad and a central deflection of about 1.5 μm. The filtering of the double exposure specklegram is done on a whole-field Fourier filtering setup (Figure 1.5). Figure 3.3 shows the fringe pattern recorded from diffraction halo A_{12} which represents the in-plane displacement component (u) of the in-plane rotation. It can be seen from the photograph that the fine fringes lie within the coarse fringes as explained in the theory. The measured sensitivity of the fine fringes is 0.9 μm, while that for the coarse fringes is 9.3 μm. In the absence of second beam illumination, the measuring sensitivity of the configuration is dependent on aperture separation.

Figures 3.4(a) and (b) show the photograph of the individual fringe patterns obtained by using one illuminating beam at a time. When both the illuminating beams are used simultaneously a moiré pattern is obtained due to the overlap of two independent fringe patterns at the observation plane. The photograph of the same when filtered via halo A_{10} and A_{20} are shown in Figures 3.5(a) and (b). In Figure 3.5(a) the fringes are due to Equation (3.7) while those in Figure 3.5(b) are due to Equation (3.8). In the moiré pattern, the horizontal lines joining the intersection points of the two fringe patterns correspond to the in-plane displacement component which is the same as that obtained from halo A_{12}. However, Figures 3.5(a) and (b) differ due to the presence of the negative sign that is associated with $\sin\alpha$ in Equation (3.7) compared to that of Equation (3.8). The influence of the $\sin\alpha$ term on the fringe pattern is very small as is evident from these photographs. This is also verified by simulating the fringe pattern using a computer.

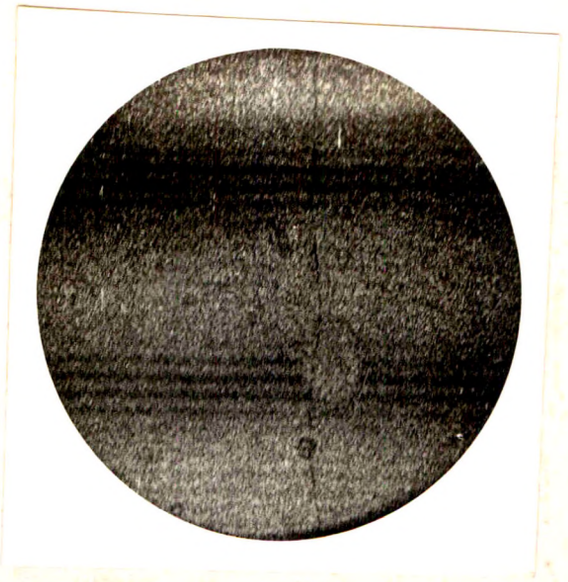

Figure 3.3 u-component of the in-plane displacement fringes of a circular diaphragm as obtained from diffraction halo A_{12}

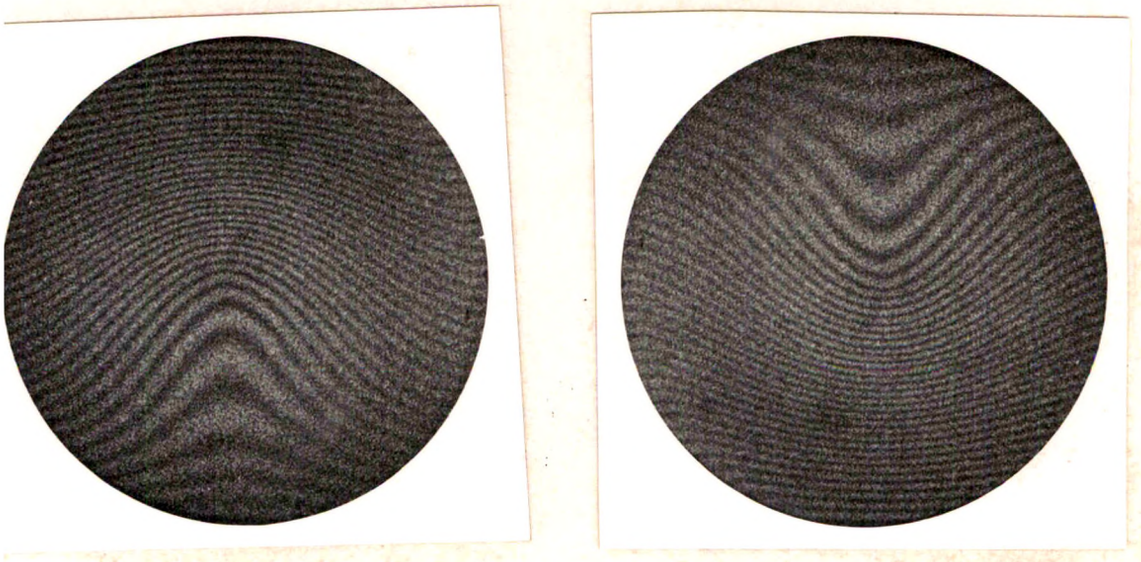

(a) (b)

Figure 3.4 (a) Fringe pattern as obtained from the diffraction halo A_{10} with the illumination beam-1

(b) Fringe pattern as obtained from the diffraction halo A_{10} with the illumination beam-2

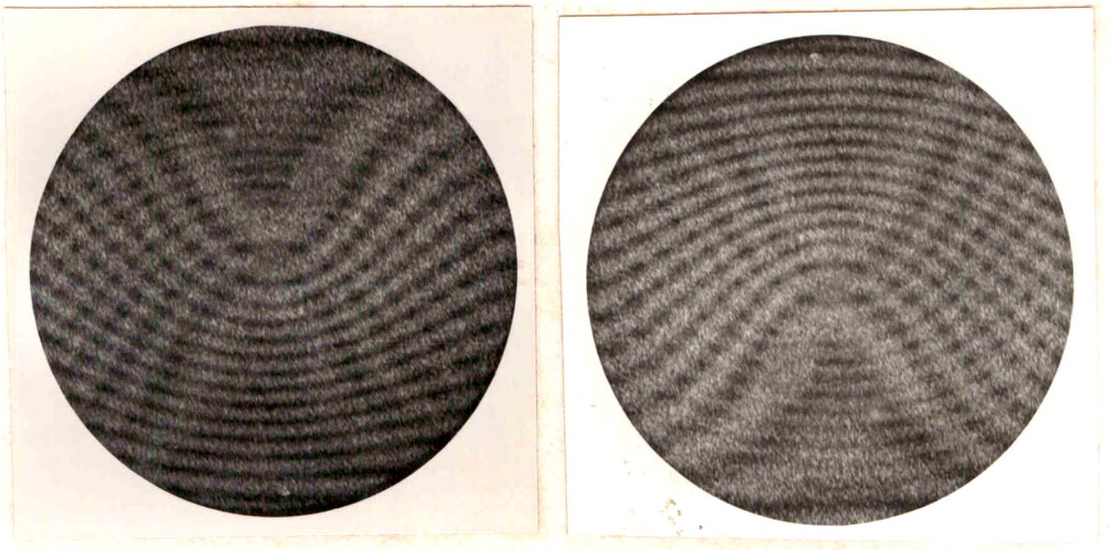

(a) (b)

Figure 3.5 (a)Moiré fringes as obtained from the diffraction halo A_{10}
(b) Moiré fringes as obtained from the diffraction halo A_{20}

From the knowledge of the magnitude of the in-plane displacement component, it is possible to obtain the out-of-plane displacement component from the resulting moiré pattern. In order to separate the in-plane and the out-of-plane displacement components from the resulting moiré pattern, the theoretical expressions for the centrally loaded diaphragm, with its edges rigidly clamped (Timoshenko and Krieger 1970a) and the experimental parameters are used to simulate the fringe patterns. The simulated fringe patterns are shown in Figure 3.6. Figures 3.6(a)–(c) are the same as that shown in Figures 3.3, 3.5(a) and (b) respectively, while the fringe pattern shown in Figure 3.6(d) is generated based on Equations (3.9) and (3.10). This shows that the influence of the $\sin\alpha$ term on the fringe pattern is considerably small and hence can be neglected for obtaining the out-of-plane displacement component from the moiré pattern. The horizontal lines joining the intersection points on Figures 3.6(b)–(d) shown by dashed lines represent the fringes due to the in-plane displacement component. The in-plane displacement data obtained either from Figure 3.6(b) or from 3.6(d) are used to extract the out-of-plane displacement component. Figures 3.7(a) and (b) show the out-of-plane displacement fringes and the corresponding 3-D plot of the object.

Thus it can be seen that with the dual beam illumination method it is possible to compute both in-plane and out-of-plane displacement components separately with comparable sensitivities from a single experiment.

3.2.5 Summary

A multi-aperture speckle interferometric method for the simultaneous measurement of in-plane and out-of-plane displacement components with nearly the same sensitivities is demonstrated. This method is supported by experimental results and computer simulated fringes.

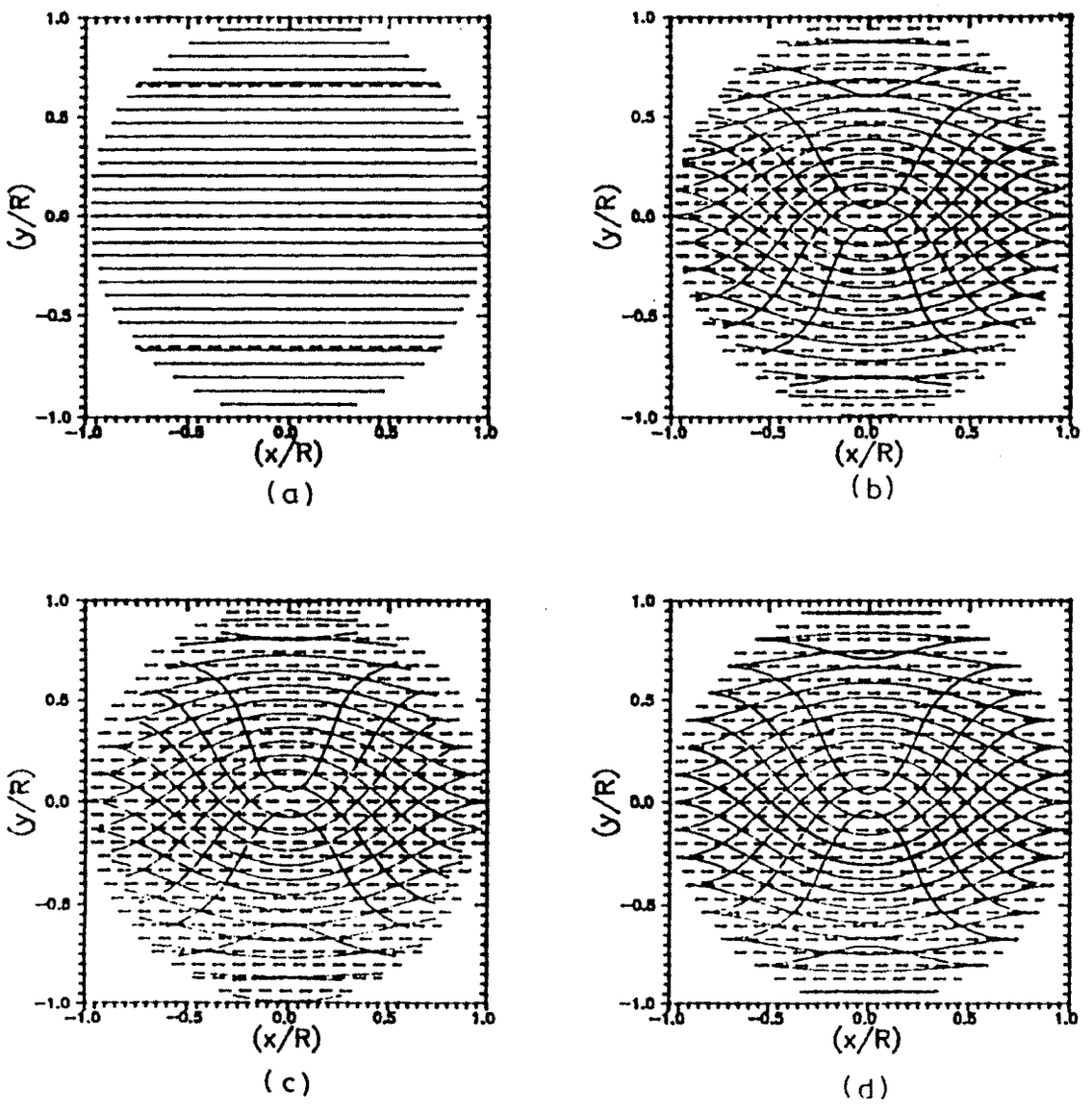

Figure 3.6(a) Simulated fringe pattern corresponding to Figure 3.3

(b) Simulated fringe pattern corresponding to Figure 3.5(a)

(c) Simulated fringe pattern corresponding to Figure 3.5(b)

(d) Simulated fringe pattern using Equations (3.9) and (3.10)

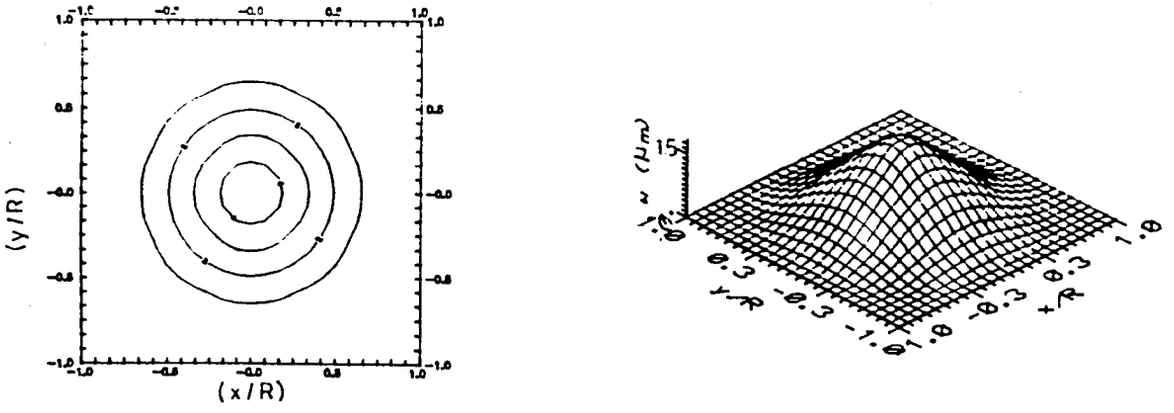

(a) (b)

Figure 3.7 (a) Separated out-of-plane deflection fringes from the moiré pattern

(b) Three dimensional plot of the out-of-plane deflection of a circular diaphragm